

Highly stable two-dimensional silicon phosphides: Different stoichiometries and exotic electronic properties

Bing Huang,^{*} Houlong L. Zhuang, Mina Yoon,[†] and Bobby G. Sumpter
Oak Ridge National Laboratory, Oak Ridge, Tennessee 37830, USA

Su-Huai Wei[‡]

National Renewable Energy Laboratory, Golden, Colorado 80401, USA

(Received 3 November 2014; revised manuscript received 13 February 2015; published 3 March 2015)

The discovery of stable two-dimensional, earth-abundant, semiconducting materials is of great interest and may impact future electronic technologies. By combining global structural prediction and first-principles calculations, we have theoretically discovered several semiconducting silicon phosphide (Si_xP_y) monolayers, which could be formed stably at the stoichiometries of $y/x \geq 1$. Interestingly, some of these compounds, i.e., $P\text{-}6m2\text{Si}_1\text{P}_1$ and $Pm\text{Si}_1\text{P}_2$, have comparable or even lower formation enthalpies than their known allotropes. The band gaps (E_g) of Si_xP_y compounds can be dramatically tuned in an extremely wide range ($0 < E_g < 3$ eV) by simply changing the number of layers. Moreover, we find that carrier doping can drive the ground state of $C2/m\text{Si}_1\text{P}_3$ from a nonmagnetic state into a robust half-metallic spin-polarized state, originating from its unique valence band structure, which can extend the use of Si-related compounds for spintronics.

DOI: [10.1103/PhysRevB.91.121401](https://doi.org/10.1103/PhysRevB.91.121401)

PACS number(s): 61.46.-w, 61.50.Ah, 61.66.Dk, 73.22.-f

The successful exfoliation of monolayer graphene opened a rapid growing research direction in condensed matter physics, that is, two-dimensional (2D) materials. In the past few years, tremendous interest has begun to focus on the search for novel 2D semiconducting materials beyond graphene. For example, 2D transition-metal dichalcogenides that have been achieved experimentally by chemical or mechanical methods [1] show interesting valley-dependent electronic properties [2] and an indirect-direct band gap transition as a function of the number of layers [1,3]. Earth-abundant silicon- and phosphorus-related compounds are extremely important for electronic and optoelectronic applications, such as transistors and solid-state lighting [4]. Very recently, silicene (monolayer silicon) [5–7] and phosphorene (monolayer black phosphorus) [8–10] have been successfully achieved in several experiments. Both silicene and phosphorene have a graphenelike honeycomb lattice but with different surface puckered structures. While silicene can only be stabilized on metal substrates [5–7], phosphorene is stable after exfoliation and could be a promising candidate for transistor applications [8–10].

The currently known earth-abundant semiconducting 2D materials are still very limited, and it is therefore highly desired to discover more of these types of materials to satisfy various electronic applications. Usually, alloying can be used to broaden or go beyond material properties of their constituent parents for specific applications. For example, (In,Ga)N alloys are critical solid-state lighting materials for different colors [11] and Cu(In,Ga)Se₂ alloys are one of three mainstream thin-film photovoltaic materials in the current market [12]. While 2D Si and P have been achieved in recent experiments, an interesting question is whether stable 2D silicon phosphide (Si_xP_y) monolayers with different stoichiometries can exist in the Si-P phase diagram. If so, what

kinds of stable stoichiometries can they have, and do they have more attractive electronic properties than that of 2D Si and P? The answers to these questions are not only scientifically important to extend our current knowledge of 2D materials, but also can provide a promising approach for the discovery of new 2D functional materials beyond the existing materials.

By combining global structural search and first-principles calculations, we have theoretically found several stable or metastable semiconducting Si_xP_y monolayers, which can only be formed at the stoichiometries of $y/x \geq 1$. Interestingly, the predicted $P\text{-}6m2\text{Si}_1\text{P}_1$ and $Pm\text{Si}_1\text{P}_2$ monolayers have similar or even lower formation enthalpies (ΔH) than their known bulk allotropes. The band gaps (E_g) of Si_xP_y compounds can be tuned in a very wide range by simply changing the number of layers. Furthermore, we find that hole doping can convert the ground state of $C2/m\text{Si}_1\text{P}_3$ from a nonmagnetic state to a robust ferromagnetic (half-metallic) state, originating from its unique valence band structure.

To find the stable 2D Si_xP_y compounds that have yet to be observed in experiments, we have conducted an unbiased structure search based on particle swarm optimization (PSO), as implemented in the CALYPSO code [13]. We focus on the different stoichiometries as Si/P ratios ranging from 3:1 (Si_3P_1) to 1:3 (Si_1P_3). For PSO predictions, any combination of numbers of atoms in the unit cell are allowed (with the total number ≤ 18 atoms). First-principles density functional theory (DFT) methods, as implemented in the VASP package [14], are used for structural relaxation and electronic structure calculations. The projector augmented wave method in conjunction with the generalized gradient approximation within the framework of Perdew-Burke-Ernzerhof is adopted for the electron exchange and correlation. The kinetic energy cutoff for the plane wave basis is set to 400 eV. A slab containing a 20 Å vacuum region in the normal direction is selected to simulate isolated 2D materials. A sufficient Γ -centered k -point mesh is carried out over the Brillouin zone for all the structures, ensuring approximately the same k -point density among different-sized supercells. All the structures are fully relaxed until the force

^{*}huangb@ornl.gov

[†]myoon@ornl.gov

[‡]Suhuai.Wei@nrel.gov

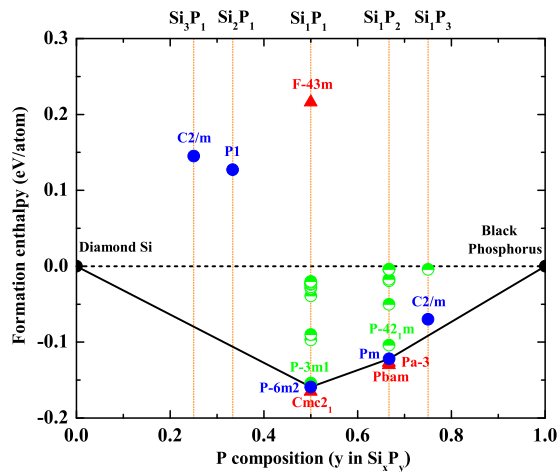


FIG. 1. (Color online) Thermodynamic stability of 2D Si_xP_y indicated by the calculated formation enthalpies (ΔH) of various 2D Si_xP_y compounds with respect to elemental decomposition into diamond silicon and black phosphorus. The solid blue circles represent the predicted lowest- ΔH Si_xP_y at each P composition. The half-solid green circles represent other predicted Si_xP_y compounds with negative ΔH values. The ground-state convex hull of 2D Si-P compounds is denoted by the solid lines. For comparison, the calculated ΔH values of four previously known bulk Si_xP_y compounds, i.e., $F-43m$ Si_1P_1 , $Cmc2_1$ Si_1P_1 , $Pbam$ Si_1P_2 , and $Pa-3$ Si_1P_2 , are also plotted as red triangles.

on each atom is less than $0.01 \text{ eV}/\text{\AA}$. It is well known that DFT underestimates the E_g of semiconductors, therefore, we have also performed accurate GW self-energy calculations [15,16] for several selected systems. To ensure the dynamical stability of our predicted structures, we use the finite displacement method, as implemented in PHONOPY code [17], to calculate the phonon frequencies.

Figure 1 summarizes the calculated formation enthalpies ΔH of various 2D Si_xP_y at different P compositions. ΔH is defined as $\Delta H = H(\text{Si}_x\text{P}_y) - xH_{\text{Si}} - yH_{\text{P}}$ and all the ΔH in Fig. 1 are given per atom at zero temperature. Thermodynamically, a Si_xP_y phase is stable or metastable against decomposition to elements if its ΔH value is negative. Diamond silicon and bulk black phosphorus, which are known to be the most stable phases of Si and P, are selected to calculate the element enthalpies of Si (H_{Si}) and P (H_{P}), respectively. When $x/y > 1$ (Si-rich condition), we cannot find any stable 2D Si_xP_y phases with negative ΔH values. The lowest- ΔH phases for $x/y = 3$ and $x/y = 2$ are $C2/m$ Si_3P_1 and $P-1$ Si_2P_1 [16], respectively. Their ΔH values are significantly positive, i.e., $0.145 \text{ eV}/\text{atom}$ for $C2/m$ Si_3P_1 and $0.127 \text{ eV}/\text{atom}$ for $P-1$ Si_2P_1 .

Interestingly, when $y/x \geq 1$, a large number of Si_xP_y monolayers with negative ΔH emerge and most of these satisfy the classical electron counting rule, i.e., Si atoms are fourfold coordinated while P atoms are threefold coordinated to realize full sp^3 hybridization. For the stoichiometry of Si_1P_1 , the lowest- ΔH phase has a GaSe-type (hexagonal, $P-6m2$) structure with $\Delta H = -0.159 \text{ eV}/\text{atom}$, as shown in Fig. 2(a). The $P-3m1$ phase [Fig. 2(b)], which shares a similar structure with the $P-6m2$ phase but with inversion

symmetry, has a negligibly higher ΔH value ($5 \text{ meV}/\text{atom}$) than that of the $P-6m2$ phase. Except for the $P-3m1$ and $P-6m2$ phases, there are nine metastable Si_1P_1 allotropes with negative ΔH values, and five compounds among them have similar structural characteristics [16]. We show one typical example in Fig. 2(c), which has $P2_1/m$ symmetry. In these five structures, the zigzag SiP chain [top view in Fig. 2(c)] is the basic building block to produce these structures. The different arrangements (numbers and orientations) of these SiP chains give rise to these five low- ΔH Si_1P_1 phases. When the P composition is further increased to the stoichiometry of Si_1P_2 , seven Si_1P_2 with negative ΔH values appear in the phase diagram. The lowest- ΔH phase has Pm symmetry with $\Delta H = -0.122 \text{ eV}/\text{atom}$. As shown in Fig. 2(d), the Pm Si_1P_2 structure can be considered as the stacking of one zigzag P chain on the h -BN-like SiP monolayer in each unit cell. The second lowest- ΔH phase is $P-42_1m$ Si_1P_2 , which has a slightly higher ΔH ($17 \text{ meV}/\text{atom}$) than that of the Pm phase. Interestingly, the Si_2P_3 pentagon is the basic building block to form the $P-42_1m$ Si_1P_2 structure, as shown in Fig. 2(e). Other negative- ΔH phases of Si_1P_2 are shown in Ref. [16]. For the stoichiometry of Si_1P_3 , we find two structures with negative ΔH , and the lowest- ΔH ($-0.069 \text{ eV}/\text{atom}$) one has $C2/m$ symmetry, as shown in Fig. 2(f). For a given stoichiometry of Si_xP_y , although there are several structures with similar ΔH , it is still possible to achieve a single crystalline Si_xP_y phase, because the diverse structural characteristics of different phases could give rise to large transition energy barriers.

The structural stabilities of these predicted structures were also checked by phonon spectrum calculations [16]. The phonon calculations demonstrate that these predicted 2D Si_xP_y structures are dynamically stable without any imaginary phonon modes. Based on the calculated ΔH values of all the 2D Si_xP_y , we can obtain the ground-state convex hull of 2D Si_xP_y , as shown in Fig. 1. Obviously, $P-6m2$ Si_1P_1 and Pm Si_1P_2 are located on the convex hull, indicating that they are stable against disproportioning into other neighboring compounds. In practice, the synthesis of a $P-6m2$ Si_1P_1 monolayer could be similar to the chemical growth of monolayer GaSe [18]. It is also important to compare the thermal stabilities of our predicted monolayer Si_xP_y to the previously known existing bulk Si_xP_y phases. Four crystalline Si_xP_y phases were reported in past experiments [19–21] and their calculated ΔH are shown in Fig. 1 (red triangles). For the stoichiometry of Si_1P_1 , the bulk $Cmc2_1$ phase has a negligibly lower ΔH value ($6 \text{ meV}/\text{atom}$) than our predicted monolayer $P-6m2$ phase, while the bulk $F-43m$ phase has a significantly positive ΔH value of $0.216 \text{ eV}/\text{atom}$. For the stoichiometry of Si_1P_2 , the predicted monolayer Pm phase also has a quite similar ΔH value (ΔH difference $< 10 \text{ meV}/\text{atom}$) as the bulk $Pbam$ and $Pa-3$ phases. It is worth noticing that despite the energy difference between diamond and graphite being as large as $\sim 20 \text{ meV}/\text{atom}$ [22], both phases can stably exist in nature. Because our calculated ΔH differences are even smaller, we believe that (at least) the predicted $P-6m2$ (and $P-3m1$) Si_1P_1 , Pm (and $P-42_1m$) Si_1P_2 , and $C2/m$ Si_1P_3 phases should be able to be formed as easily as their existing allotropes, at least under nonequilibrium growth conditions, by carefully selecting specific substrates. They might also exist in nature but have not yet been discovered.

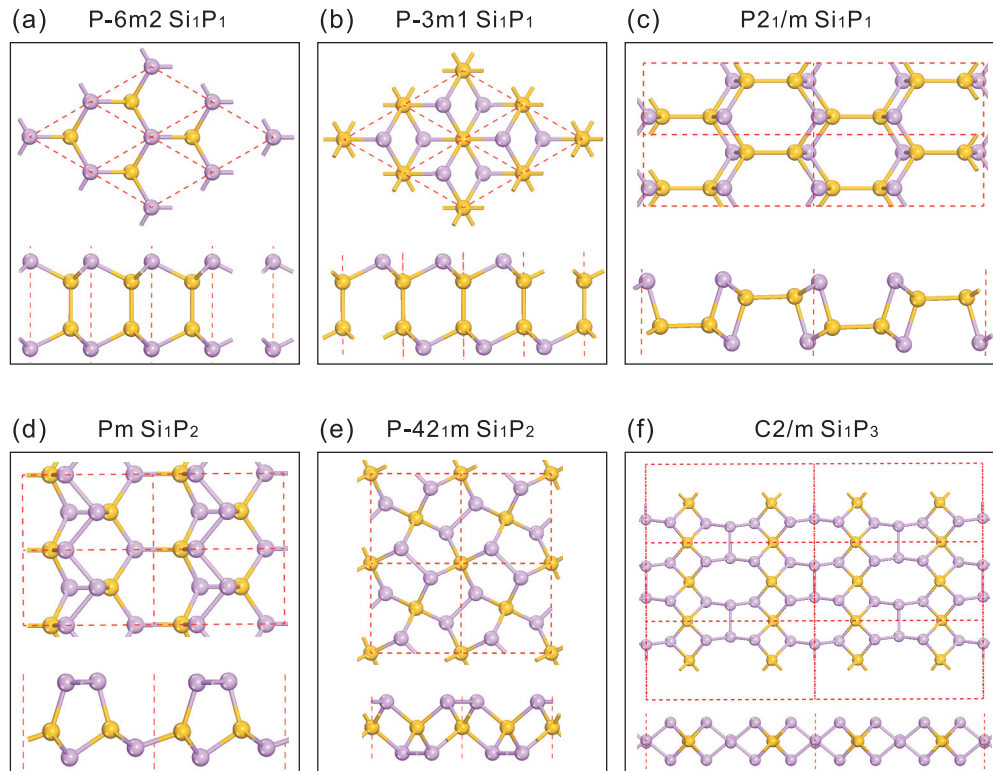


FIG. 2. (Color online) Structures of 2D Si_xP_y . The top view (upper) and side view (lower) of (a) $P\text{-}6m2\text{Si}_1\text{P}_1$, (b) $P\text{-}3m1\text{Si}_1\text{P}_1$, (c) $P2_1/m\text{Si}_1\text{P}_1$, (d) $Pm\text{Si}_1\text{P}_2$, (e) $P\text{-}42_1m\text{Si}_1\text{P}_2$, and (f) $C2/m\text{Si}_1\text{P}_3$. Violet and yellow spheres are P and Si atoms, respectively. The unit cells are marked by the red dashed lines.

The DFT-calculated band structures of these 2D Si_xP_y compounds are shown in Fig. 3. As shown in Fig. 3(a), $P\text{-}6m2\text{Si}_1\text{P}_1$ is an indirect gap semiconductor with E_g of 1.54 eV. The valence band maximum (VBM) is contributed by the hybridized $3p$ (π) orbitals from P and Si atoms, while the conduction band minimum (CBM) is contributed by the hybridized $3s$ and $3p$ orbitals of Si and P atoms. Interestingly, we find that the valence band dispersion around the Fermi level (E_F) in this structure is similar to that of GaSe [18,23]. This unusual flat valence band dispersion around the Γ point and E_F gives rise to a rather high DOS and a van Hove singularity around the VBM. The more accurate $GW\text{-}E_g$ of $P\text{-}6m2\text{Si}_1\text{P}_1$

is 2.61 eV, and the band dispersion around E_F is close to that of the DFT results [16]. The band structure of $P\text{-}3m1\text{Si}_1\text{P}_1$ is similar to the $P\text{-}6m2$ one [16], and the DFT (GW) E_g is 1.78 (2.97) eV. Comparing to the calculated $GW\text{-}E_g$, we can estimate that the DFT- E_g of the Si_xP_y monolayer is roughly underestimated by ~ 1.1 eV. $P2_1/m\text{Si}_1\text{P}_1$ is a direct gap semiconductor with a DFT- E_g of 1.05 eV at the Γ point. Its VBM is contributed by the Si-P $3p$ (σ) orbitals, while CBM is contributed by the Si $3p$ (π) and $3s$ orbitals [Fig. 3(b)]. As shown in Fig. 3(c), $Pm\text{Si}_1\text{P}_2$ is a (quasi)direct semiconductor with a DFT- E_g of 1.58 eV. Its VBM is mainly contributed by the P $3p$ states, while its CBM is mainly contributed by the

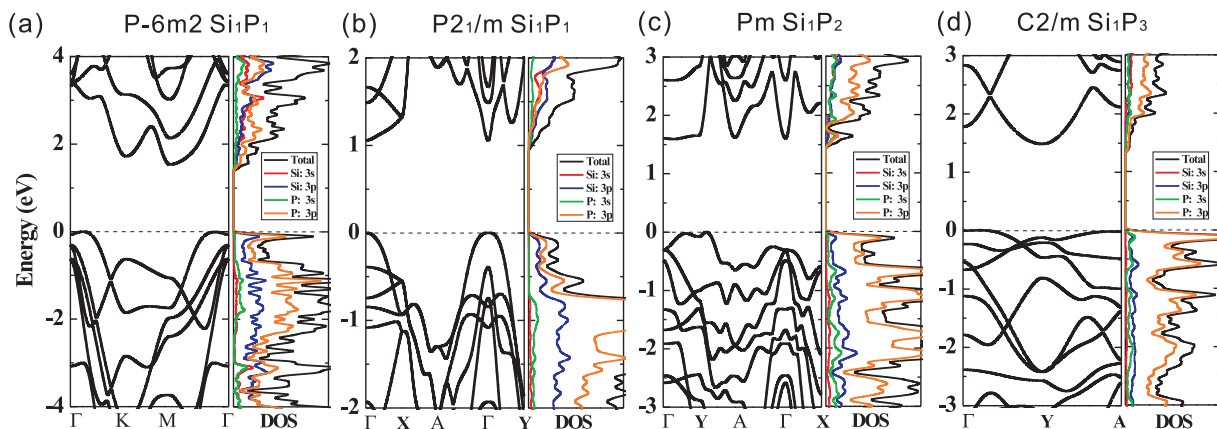


FIG. 3. (Color online) Electronic structures of 2D Si_xP_y . The DFT-calculated band structures of (a) $P\text{-}6m2\text{Si}_1\text{P}_1$, (b) $P2_1/m\text{Si}_1\text{P}_1$, (c) $Pm\text{Si}_1\text{P}_2$, and (d) $C2/m\text{Si}_1\text{P}_3$. The total and partial density of states (DOS) of these structures are also plotted in (a)–(d). The Fermi level is set to zero.

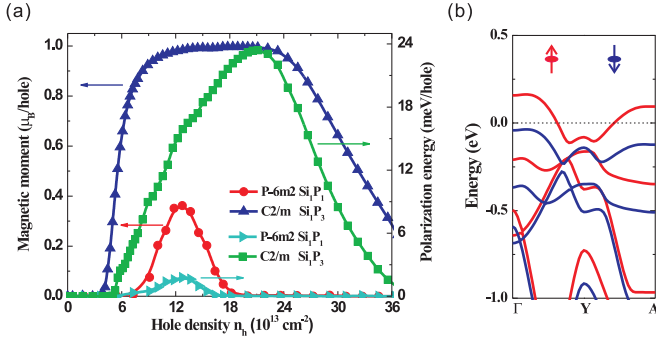


FIG. 4. (Color online) Magnetic properties of 2D Si_xP_y . (a) The magnetic moments and spin polarization energies of 2D $P\text{-}6m2\text{Si}_1\text{P}_1$ and $C2/m\text{Si}_1\text{P}_3$ as a function of carrier (hole) density n_h . (b) The DFT-calculated (valence) band structure of $C2/m\text{Si}_1\text{P}_3$ at $n_h = 1.5 \times 10^{14} \text{ cm}^{-2}$. The spin-up and spin-down bands are shown as red and blue colors, respectively. The Fermi level is set to zero.

$P\ 3s$ and $3p$ orbitals. $P\text{-}421m\text{Si}_1\text{P}_2$ [Fig. 2(e)] is an indirect semiconductor with a DFT- E_g of 1.89 eV [16]. $C2/m\text{Si}_1\text{P}_3$ [Fig. 3(d)] is a weakly indirect gap semiconductor with a DFT- E_g of 1.49 eV. Its minimum direct gap (1.61 eV) is located at the Y point. The VBM is mostly contributed by the $P\ 3p$ (π) state and CBM is mainly contributed by the hybridized $P\ 3s$ and $3p$ orbitals. This unique atomic nonbondinglike character of $P\ 3p$ states around VBM results in an extremely high DOS and van Hove singularity. The DFT- E_g of other metastable Si_xP_y (with negative ΔH) are in a wide range of 0.49–1.80 eV [16].

According to the Stoner criterion, spontaneous ferromagnetism could appear if the exchange splitting energy is larger than the loss in kinetic energy, i.e., if the DOS at E_F is high enough [24,25]. Since $P\text{-}6m2\text{Si}_1\text{P}_1$ [Fig. 3(a)] and $C2/m\text{Si}_1\text{P}_3$ [Fig. 3(d)] have very large DOS around the VBM, by doping holes into these two systems, one can shift the E_F to a position with high DOS so that it may satisfy the Stoner criterion. The spin polarization energy (E_p), defined by the energy difference between the spin-polarized state and non-spin-polarized state, was calculated to check the stability of spin polarization. As expected, these two systems can indeed be converted into a ferromagnetic ground

state at critical hole densities (n_h), as shown in Fig. 4(a). For $P\text{-}6m2\text{Si}_1\text{P}_1$, the range of $0.20\text{--}0.40\mu_B/\text{hole}$ can be achieved when $1 \times 10^{14} < n_h < 1.6 \times 10^{14} \text{ cm}^{-2}$. However, the maximum E_p of Si_1P_1 is $\leq 2 \text{ meV}/\text{hole}$, which means that an extremely low temperature is necessary to stabilize the spin polarization. Interestingly, $C2/m\text{Si}_1\text{P}_3$ has a much stronger spin polarization effect upon hole doping, which is consistent with the fact that the DOS around VBM in $C2/m\text{Si}_1\text{P}_3$ is about six times higher than that of $P\text{-}6m2\text{Si}_1\text{P}_1$. As shown in Fig. 4(a), the spin moment in $C2/m\text{Si}_1\text{P}_3$ is rapidly increasing when $n_h > 4 \times 10^{13} \text{ cm}^{-2}$, as the DOS at E_F in the system is increasing. The system finally reaches a plateau of $\sim 1\mu_B/\text{hole}$ when $8 \times 10^{13} < n_h < 2.5 \times 10^{14} \text{ cm}^{-2}$. As an example, Fig. 4(b) shows the band structure of Si_1P_3 at $n_h = 1.5 \times 10^{14} \text{ cm}^{-2}$. Here, the system now behaves as an ideal half-metallic phase, i.e., 100% spin polarization around E_F . When $n_h > 2.5 \times 10^{14} \text{ cm}^{-2}$, the spin moment gradually decreases as the DOS at E_F decreases. Remarkably, we find that E_p could be significantly high ($> 10 \text{ meV}/\text{hole}$) in a wide range of n_h ($8 \times 10^{13} < n_h < 3 \times 10^{14} \text{ cm}^{-2}$), indicating that the ferromagnetic states are very stable, which is important for practical applications. This is also a prediction that half metallicity could be achieved in 2D Si- and P-based compounds. It is worth noting that high carrier densities have already been experimentally achieved in other monolayer materials by applying gate voltages, such as graphene ($4 \times 10^{14} \text{ cm}^{-2}$) [26] and MoS_2 ($2 \times 10^{14} \text{ cm}^{-2}$) [27].

It is also interesting to understand the thickness effects on the electronic properties of these 2D Si_xP_y . We select $P\text{-}6m2\text{Si}_1\text{P}_1$ as an example to study the E_g as a function of the number of layers (N). Just as for GaSe [28], Si_1P_1 layers can form four different bulk crystal structures, i.e., β -, ϵ -, γ -, and δ - Si_1P_1 . The β stacking [$P6_3/mmc$, inset of Fig. 5(a)] has a negligibly lower energy than other stacking types [29]. Surprisingly, as N increases, DFT- E_g is dramatically decreased from 1.54 eV (monolayer) to 0 eV (negative E_g). The more accurate GW calculations also confirm that the E_g of bulk β - Si_1P_1 is $\sim 0 \text{ eV}$ [16]. Importantly, our calculations also demonstrate that this N -dependent metal-insulator transition is very robust and generally exists in the ϵ -, γ -, and δ -stacking Si_1P_1 systems. The N -dependent E_g is much more noticeable

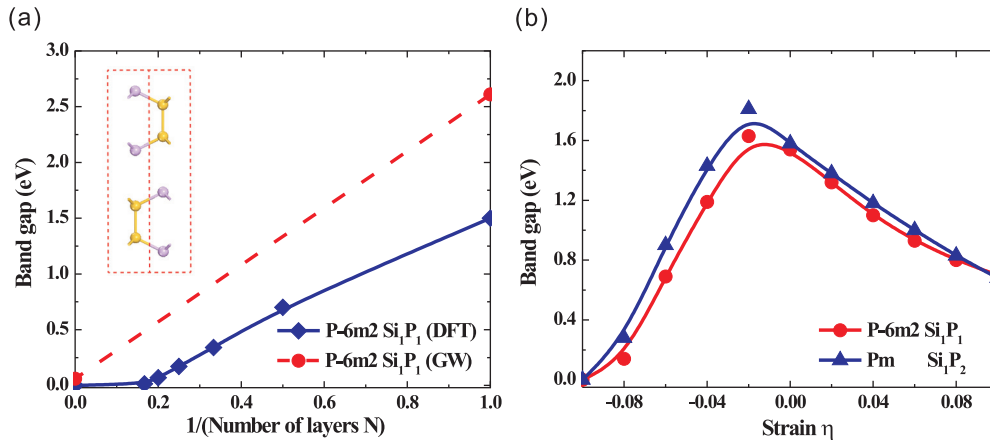


FIG. 5. (Color online) Thickness- and strain-dependent electronic properties of 2D Si_xP_y . (a) The DFT and GW calculated band gaps of $P\text{-}6m2\text{Si}_1\text{P}_1$ as a function of the number of layers. The dashed lines connect the band gaps corrected by GW calculation. Inset: The side view of the structure of bulk β - Si_1P_1 . (b) The DFT calculated band gaps of $P\text{-}6m2\text{Si}_1\text{P}_1$ and $Pm\text{Si}_1\text{P}_2$ monolayers as a function of in-plane strain η .

than that in MoS₂ and GaSe [1,3,18], which could be attractive for applications where the metal-insulator transition is desired.

Finally, we find that an in-plane strain η can also dramatically change E_g and even its characters from direct (indirect) to indirect (direct) in 2D Si_xP_y, similar to pure phosphorene layers [8,30]. For example, a large η can significantly reduce the E_g of monolayer Si₁P₁ and Si₁P₂ [Fig. 5(b)]. Especially, when $\eta < -2\%$, Si₁P₂ is converted from a direct gap semiconductor to an indirect one, which could be very useful for optical applications.

In conclusion, we have theoretically identified several stable or metastable semiconducting Si_xP_y monolayers. As the different family members of 2D materials, these Si_xP_y monolayers not only have significantly different structures compared to their constituent parents, but also show very unusual and promising electronic (e.g., metal-insulator

transition) and magnetic (e.g., half-metallicity) properties beyond their constituent parents. More generally, our study provides an experimentally achievable idea to discover functional 2D materials, via alloying, for broader electronic applications.

The work at ORNL was supported by the Scientific User Facilities Division (B.G.S., M.Y.) and the Materials Science and Engineering Division (B.H., H.L.Z.), Basic Energy Sciences, US Department of Energy. The research at NREL (S.H.W.) was sponsored by the US Department of Energy under Contract No. DE-AC36-08GO28308. Computing resources were provided by the Leadership Computing Facility at Oak Ridge National Laboratory and the National Energy Research Scientific Computing Center, which is supported by the Office of Science of the US Department of Energy under Contract No. DE-AC02-05CH11231.

-
- [1] Q. H. Wang, K. Kalantar-Zadeh, A. Kis, J. N. Coleman, and M. S. Strano, *Nat. Nanotechnol.* **7**, 699 (2012).
- [2] X. Xu, W. Yao, D. Xiao, and T. F. Heinz, *Nat. Phys.* **10**, 343 (2014).
- [3] K. F. Mak, C. Lee, J. Hone, J. Shan, and T. F. Heinz, *Phys. Rev. Lett.* **105**, 136805 (2010).
- [4] M. Peruzzini and L. Gonsalvi, *Phosphorus Compounds: Advanced Tools in Catalysis and Material Sciences* (Springer, Berlin, 2011).
- [5] P. Vogt, P. De Padova, C. Quaresima, J. Avila, E. Frantzeskakis, M. C. Asensio, A. Resta, B. Ealet, and G. L. Lay, *Phys. Rev. Lett.* **108**, 155501 (2012).
- [6] L. Chen, C.-C. Liu, B. Feng, X. He, P. Cheng, Z. Ding, S. Meng, Y. Yao, and K. Wu, *Phys. Rev. Lett.* **109**, 056804 (2012).
- [7] A. Fleurence, R. Friedlein, T. Ozaki, H. Kawai, Y. Wang, and Y. Yamada-Takamura, *Phys. Rev. Lett.* **108**, 245501 (2012).
- [8] H. Liu, A. T. Neal, Z. Zhu, Z. Luo, X. Xu, D. Tománek, and P. D. Ye, *ACS Nano* **8**, 4033 (2014).
- [9] S. P. Koenig, R. A. Doganov, H. Schmidt, A. H. Castro Neto, and B. Ozyilmaz, *Appl. Phys. Lett.* **104**, 103106 (2014).
- [10] L. Li, Y. Yu, G. J. Ye, Q. Ge, X. Ou, H. Wu, D. Feng, X. H. Chen, and Y. Zhang, *Nat. Nanotechnol.* **9**, 373 (2014).
- [11] A. Bergh, G. Craford, A. Duggal, and R. Haitz, *Phys. Today* **54** (12), 42 (2001).
- [12] P. Jackson, D. Hariskos, E. Lotter, S. Paetel, R. Wuerz, R. Menner, W. Wischmann, and M. Powalla, *Prog. Photovoltaics* **19**, 894 (2011).
- [13] Y. Wang, J. Lv, L. Zhu, and Y. Ma, *Phys. Rev. B* **82**, 094116 (2010).
- [14] G. Kresse and J. Furthmüller, *Comput. Mater. Sci.* **6**, 15 (1996).
- [15] M. S. Hybertsen and S. G. Louie, *Phys. Rev. B* **34**, 5390 (1986); L. Wirtz, A. Marini, and A. Rubio, *Phys. Rev. Lett.* **96**, 126104 (2006); C.-H. Park, C. D. Spataru, and S. G. Louie, *ibid.* **96**, 126105 (2006).
- [16] See Supplemental Material at <http://link.aps.org/supplemental/10.1103/PhysRevB.91.121401> for additional information regarding other metastable Si_xP_y, GW calculation methods and results, phonon spectra of Si_xP_y, and electronic structures of Si_xP_y as a function of strain or thickness.
- [17] A. Togo, F. Oba, and I. Tanaka, *Phys. Rev. B* **78**, 134106 (2008).
- [18] X. Li, W. Lin, A. Puzdsky, J. C. Idrobo, C. Ma, M. Chi, M. Yoon, C. M. Rouleau, I. I. Kravchenko, D. B. Geohegan, and K. Xiao, *Sci. Rep.* **4**, 5497 (2014).
- [19] J. Osugi, R. Namikawa, and Y. Tanaka, *Rev. Phys. Chem. Jpn.* **36**, 35 (1966).
- [20] P. C. Donohue, W. J. Siemons, and J. L. Gillson, *J. Phys. Chem. Solids* **29**, 807 (1968).
- [21] T. Wadsten, *Chem. Commun.* **7**, 1 (1973).
- [22] P. Hawtin, J. B. Lewis, M. Moul, and R. H. Philips, *Philos. Trans. R. Soc. London, Ser. A* **261**, 67 (1966).
- [23] V. Zolyomi, N. D. Drummond, and V. I. Falko, *Phys. Rev. B* **87**, 195403 (2013).
- [24] B. Huang, F. Liu, J. Wu, B.-L. Gu, and W. H. Duan, *Phys. Rev. B* **77**, 153411 (2008).
- [25] H. Peng, H. J. Xiang, S.-H. Wei, S.-S. Li, J.-B. Xia, and J. Li, *Phys. Rev. Lett.* **102**, 017201 (2009).
- [26] D. K. Efetov and P. Kim, *Phys. Rev. Lett.* **105**, 256805 (2010).
- [27] J. T. Ye, Y. J. Zhang, R. Akashi, M. S. Bahramy, R. Arita, and Y. Iwasa, *Science* **338**, 1193 (2012).
- [28] A. Kuhn, A. Chevy, and R. Chevalier, *Phys. Status Solidi A* **31**, 469 (1975).
- [29] The van de Waals interactions are described using the optB86-vdW functional [J. Klimes, D. R. Bowler, and A. Michaelides, *Phys. Rev. B* **83**, 195131 (2011)].
- [30] Z. Zhu and D. Tománek, *Phys. Rev. Lett.* **112**, 176802 (2014); J. Guan, Z. Zhu, and D. Tománek, *ibid.* **113**, 046804 (2014).